



Permeability of Bituminous Coal to CH₄ and CO₂ Under Fixed Volume and Fixed Stress Boundary Conditions: Effects of Sorption

Jinfeng Liu^{1,2,3*} and Christopher J. Spiers⁴

¹School of Earth Sciences and Engineering, Sun Yat-Sen University, Guangzhou, China, ²Guangdong Provincial Key Lab of Geodynamics and Geohazards, Sun Yat-Sen University, Guangzhou, China, ³Southern Marine Science and Engineering Guangdong Laboratory, Zhuhai, China, ⁴Department of Earth Sciences, Utrecht University, Utrecht, Netherlands

OPEN ACCESS

Edited by:

Jienan Pan,
Henan Polytechnic University, China

Reviewed by:

YanJun Meng,
Taiyuan University of Technology,
China
Yinbo Zhou,
Henan University of Engineering,
China
Gaofeng Liu,
Henan Polytechnic University, China

*Correspondence:

Jinfeng Liu
liujinf5@mail.sysu.edu.cn

Specialty section:

This article was submitted to
Economic Geology,
a section of the journal
Frontiers in Earth Science

Received: 16 February 2022

Accepted: 30 March 2022

Published: 09 May 2022

Citation:

Liu J and Spiers CJ (2022) Permeability of Bituminous Coal to CH₄ and CO₂ Under Fixed Volume and Fixed Stress Boundary Conditions: Effects of Sorption. *Front. Earth Sci.* 10:877024. doi: 10.3389/feart.2022.877024

Permeability evolution in coal reservoirs during CO₂-enhanced coalbed methane (ECBM) production is strongly influenced by swelling/shrinkage effects related to sorption and desorption of CO₂ and CH₄, respectively. Recent research has demonstrated fully coupled stress–strain–sorption–diffusion behavior in small samples of cleat-free coal matrix material exposed to a sorbing gas. However, it is unclear how such effects influence permeability evolution at the scale of a cleated coal seam and whether a simple fracture permeability model, such as the Walsh elastic asperity loading model, is appropriate. In this study, we performed steady-state permeability measurements, to CH₄ and CO₂, on a cylindrical sample of highly volatile bituminous coal (25 mm in diameter) with a clearly visible cleat system, under (near) fixed volume versus fixed stress conditions. To isolate the effect of sorption on permeability evolution, helium (non-sorbing gas) was used as a control fluid. All flow-through tests reported here were conducted under conditions of single-phase flow at 40°C, at applied Terzaghi effective confining pressures of 14–41 MPa. Permeability evolution versus effective stress data were obtained under both fixed volume and fixed stress boundary conditions, showing an exponential correlation. Importantly, permeability (κ) obtained at similar Terzaghi effective confining pressures showed $\kappa_{\text{helium}} > \kappa_{\text{CH}_4} \gg \kappa_{\text{CO}_2}$, while κ -values measured in the fixed volume condition were higher than those in the fixed stress case. The results show that permeability to CH₄ and CO₂, under *in situ* conditions where free swelling of rock is not possible, is strongly influenced by the coupled effects of 1) self-stress generated by constrained swelling, 2) the change in effective stress coefficient upon sorption, 3) sorption-induced closure of transport paths independently of poroelastic effect, and 4) heterogeneous gas penetration and equilibration, dependent on diffusion. Our results also show that the Walsh permeability model offers a promising basis for relating permeability evolution to *in situ* stress evolution, using appropriate parameter values corrected for the effects of stress–strain–sorption.

Keywords: adsorption-induced swelling, swelling stress, Walsh effective stress, transport paths, diffusion and equilibrium, CO₂-ECBM

INTRODUCTION

Subsurface coal seams typically consist of nanoporous coal matrix material, within which gas adsorption/desorption and diffusion mainly occur, cut by a multiscale network of joints or cleats that act as the main transport paths for gas flow (e.g., Levine, 1996; Laubach et al., 1998; Moore, 2012). Coal seam permeability is widely accepted as the most important factor for assessing the economic feasibility of (CO₂) enhanced coalbed methane (ECBM) recovery, playing a significant role in ECBM recovery and reservoir modeling (e.g., Moore, 2012). At fixed gas or fluid pressure, fracture or cleat permeability of coal samples is strongly sensitive to the Terzaghi effective normal stress (confining pressure) or (Terzaghi) effective stress, i.e., the difference between confining pressure (P_c) and pore fluid pressure (P_f) acting on the sample, decreasing rapidly with increasing Terzaghi effective stress at a rate that depends on initial permeability and the stresses employed (e.g., Somerton et al., 1975; Durucan and Edwards, 1986; Chen et al., 2011; Gensterblum et al., 2014). At the same time, adsorption or desorption of CH₄/CO₂ by coal matrix material due to an increase or decrease in gas/fluid pressure at constant effective stress can cause swelling or shrinkage by several percent (e.g., Levine, 1996; Karacan, 2007; Day et al., 2012; Hol and Spiers, 2012; Liu et al., 2016), also affecting strongly the evolution of fracture permeability in coal seams. Many field pilots and laboratory experiments investigating ECBM production have further demonstrated that the net swelling of coal caused by CH₄ displacement by injected CO₂ causes an increase in the mean stress under confined subsurface conditions, simply closing transport paths and reducing coal seam permeability (van Bergen et al., 2006; Pini et al., 2009; Fujioka et al., 2010; Kiyama et al., 2011). Much attention has therefore been paid to understanding how these effects interact and how the permeability of coal samples develops during sorption of gases, such as N₂, CH₄, and CO₂ (e.g., Palmer, 2009; Liu et al., 2011a; Liu et al., 2011b; Pan and Connell, 2012; Zhou et al., 2013; Shi et al., 2018). The main findings from experiments and models may be summarized as follows.

First, sorption-induced swelling or desorption-induced shrinkage occurring under fixed volume boundary conditions causes the changes in stress state, involving (poro)elastic or plastic deformation or even failure (Espinoza et al., 2014; Espinoza et al., 2015; Espinoza et al., 2016). This can accordingly lead to a change in permeability (Wang et al., 2013; Espinoza et al., 2015; Zhu et al., 2018).

Second, sorption-induced swelling behavior may change the mechanical properties of coal. These effects include 1) a change in elastic compressibility or bulk modulus upon microcracking caused by diffusion-controlled heterogeneous sorption (Gensterblum et al., 2014; Hol et al., 2014; Hol et al., 2012b; Karacan, 2003; Liu et al., 2017; Wu et al., 2011) and 2) an apparent change in Biot effective stress coefficient caused by competition between the change in compressibility and adsorption-induced swelling (Liu and Harpalani, 2014; Sang et al., 2017). Note here that the apparent Biot effective stress coefficient upon adsorption of CH₄ or CO₂ may be greater than 1.

Third, diffusion-controlled sorption processes can cause permeability evolution even at a fixed effective stress (Chen et al., 2011; Liu et al., 2011c; Chen et al., 2012; Peng et al., 2014; Zang and Wang, 2017; Wang et al., 2021). This can be related to the changes in the degree of sorption as equilibrium is approached (Chen et al., 2011; Liu et al., 2011c; Chen et al., 2012; Peng et al., 2014; Liu et al., 2017), or to changes in transport paths (Brown and Scholz, 1985, 1986; Zimmerman et al., 1992) that may in turn be caused by changes in fracture surface roughness, contact area, and aperture during sorption (Hol et al., 2014; Wang et al., 2017).

Fourth, experiments and thermodynamics have demonstrated the applied stress could reduce adsorption capacity for CO₂ and CH₄ by 5–50% (Pone et al., 2009; Hol et al., 2011; Hol et al., 2012a; Liu et al., 2016), thus changing sorption-induced swelling strain (Pan and Connell, 2007; Vandamme et al., 2010). This suggests that a fully coupled stress–strain–sorption process occurring in subsurface coal, which also has an impact on diffusion of gas/fluid molecules in the nanoporous coal matrix (Liu et al., 2017), has to be considered.

However, it remains unclear how the coupled stress–strain–sorption effects influence coal seam permeability *via* the likely mechanisms described above in the first to the third case, particularly under subsurface confined boundary conditions. In this study, we attempt to determine how the coupled stress–strain–sorption behavior occurring at *in situ* subsurface boundary conditions, where swelling is constrained by the surrounding rock mass, influences permeability evolution and whether this permeability evolution can be adequately quantified in the simple elastic asperity loading model for crack closure developed by Walsh (1981). To achieve this, flow-through tests were performed on a cored bituminous coal sample to measure permeability evolution during flow-through of helium, CH₄, and CO₂, under both fixed volume and fixed stress boundary conditions. The influence of effective normal stresses on permeability was compared with the Walsh permeability model. On this basis, we discuss the likely mechanisms and effects of stress–strain–sorption on the Walsh effective stress coefficient for permeability and on the internal structure of the transport paths carrying gas/fluid flow. Finally, the implications of our findings for (CO₂) ECBM recovery are discussed.

EXPERIMENTAL ASPECTS

We performed measurements of permeability to CH₄ and CO₂, under either (near) fixed volume or fixed stress boundary conditions. The tests were performed on a cylindrical sample of highly volatile bituminous coal (25 mm in diameter) with a clearly visible cleat system (see **Figure 1**), using the steady-state flow method. Helium (non-sorbing gas) was used as a control fluid, in an attempt to isolate the effect of sorption on permeability evolution. All measurements were conducted under conditions of single-phase flow at 40°C, using the purpose-designed apparatus shown in **Figure 2**.

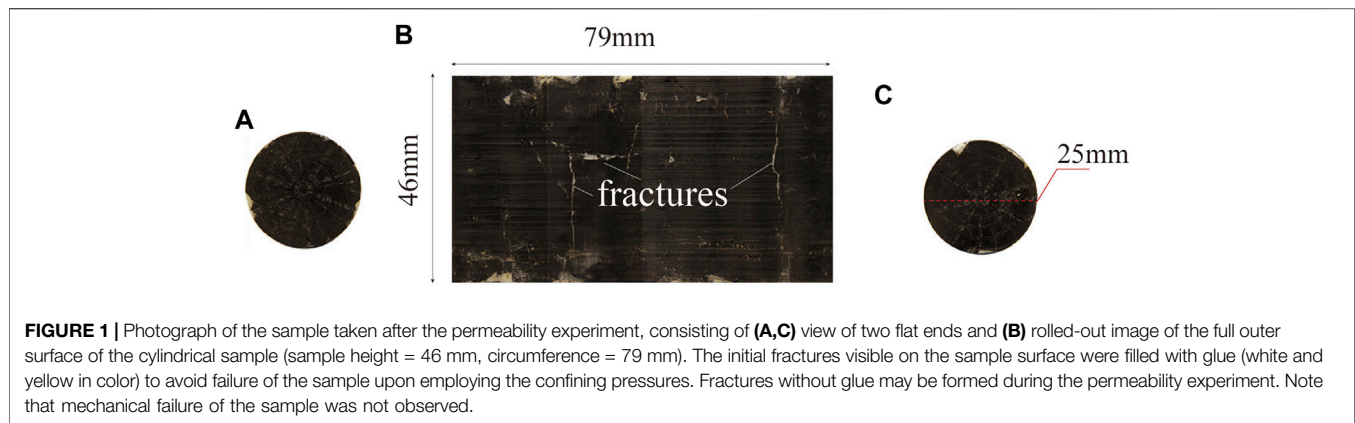


FIGURE 1 | Photograph of the sample taken after the permeability experiment, consisting of (A,C) view of two flat ends and (B) rolled-out image of the full outer surface of the cylindrical sample (sample height = 46 mm, circumference = 79 mm). The initial fractures visible on the sample surface were filled with glue (white and yellow in color) to avoid failure of the sample upon employing the confining pressures. Fractures without glue may be formed during the permeability experiment. Note that mechanical failure of the sample was not observed.

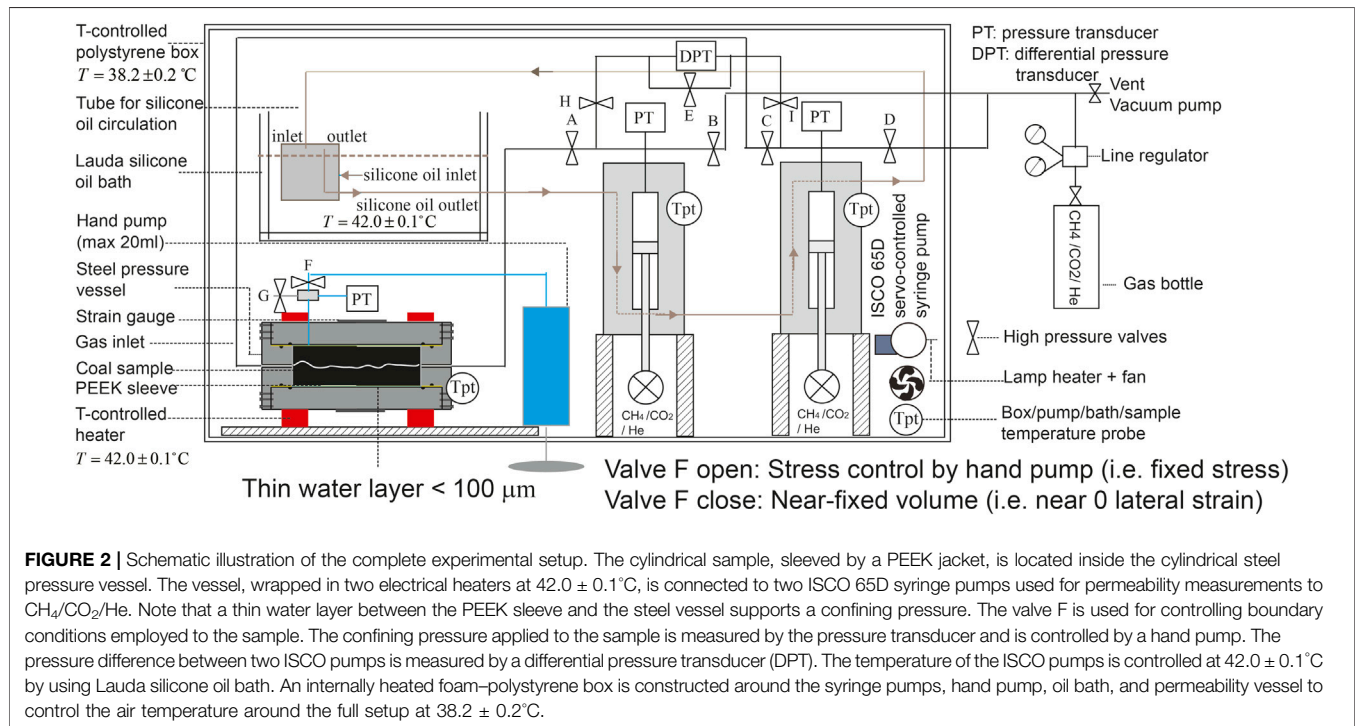


FIGURE 2 | Schematic illustration of the complete experimental setup. The cylindrical sample, sleeved by a PEEK jacket, is located inside the cylindrical steel pressure vessel. The vessel, wrapped in two electrical heaters at $42.0 \pm 0.1^\circ\text{C}$, is connected to two ISCO 65D syringe pumps used for permeability measurements to $\text{CH}_4/\text{CO}_2/\text{He}$. Note that a thin water layer between the PEEK sleeve and the steel vessel supports a confining pressure. The confining pressure applied to the sample is measured by the pressure transducer and is controlled by a hand pump. The pressure difference between two ISCO pumps is measured by a differential pressure transducer (DPT). The temperature of the ISCO pumps is controlled at $42.0 \pm 0.1^\circ\text{C}$ by using Lauda silicone oil bath. An internally heated foam-polystyrene box is constructed around the syringe pumps, hand pump, oil bath, and permeability vessel to control the air temperature around the full setup at $38.2 \pm 0.2^\circ\text{C}$.

Sample Preparation and Treatment

The sample material used consisted of highly volatile bituminous coal collected from Brzeszcze 364, Poland. The Brzeszcze coal has a vitrinite reflectance of $0.77 \pm 0.05\%$ and contains 74.1% carbon, 5.3% hydrogen, 1.4% nitrogen, 0.7% sulfur, and 18.5% oxygen (Hol et al., 2011). Specifically, the Brzeszcze coal contains 2.9% moisture content and 5.2% ash content. We prepared a single cylindrical sample of the Brzeszcze coal measuring 25 mm in diameter by 45.84 mm in length, cored normal to bedding (see Figure 1). Note that the sample contains a visible multiscale network of cleats. The mass and the bulk volume of the sample, measured before the permeability test, were 28.02 g and 22.49 ml, respectively. Taking 1.45 g/ml as the matrix/grain density of the Brzeszcze coal (Hol and Spiers, 2012), calculation of the initial porosity of the sample used in this study yields $\sim 14\%$.

After evacuation, the sample was pre-treated with CH_4 to allow equilibration under fixed volume boundary conditions, employing 10 MPa fluid pressure and an initial confining pressure of 11 MPa. This took around 5 days and produced a maximum self-swelling stress of 30.7 MPa. The sample was then evacuated for several days for gas desorption and was then kept in a vacuum oven for a month before starting the experiment. Note that microfractures might be formed during this treatment, speeding up gas diffusion and adsorption equilibration during the experiment (Hol et al., 2012a).

Apparatus

The apparatus used in the present experiment (Figure 2) consisted of a stainless steel pressure vessel, housing the jacketed sample and wrapped in two temperature-controlled

TABLE 1 | Experimental lists indicating the working fluid, boundary conditions, mean pore fluid pressure (P_c) employed in the flow-through tests, pressure difference between upstream and downstream (P_u-P_d), and confining pressure (P_c) employed at fixed stress for each stage.

Stages	I	II	III	IV	V
Working fluid	He	CH ₄	He	CO ₂	He
Fixed volume	—	✓	—	✓	—
Fixed stress	✓	✓	✓	✓	✓
P_f (MPa)	3.2–9.2	3.2–10.2	3.2–9.2	11–15	3.2–9.2
P_u-P_d (MPa)	0.4	0.4	0.4	2	0.4
P_c (MPa)	18–38	17–37	18–38	25–40	18–38

electrical heaters maintained at $42.0 \pm 0.1^\circ\text{C}$. The ends of the sample were fully attached to the closure nuts of the steel vessel, sealed using O-rings against the inner PEEK jacket. The two closure nuts and the sample assembled inside the jacket were fixed to the steel vessel using screws, sealed using O-rings against the inner vessel wall, i.e., the sample was subjected to a fixed displacement in the axial direction. The jacketed sample was pressurized externally (radially compressed) as P_c , via a thin water layer ($<100 \mu\text{m}$) inside the vessel, using water as a confining fluid, driven by a hand volumetric pump and measured by an independent pressure transducer. The high pressure valve F (**Figure 2**) is used for achieving constant volume (close) or fixed stress (open) boundary conditions. Gas was introduced into the sample via a high pressure line passing through the closure nut of the steel vessel. The gas flow-through was controlled by two independent ISCO 65D volumetric (syringe) pumps (cf. Hol and Spiers, 2012). Both ISCO pumps were operated in constant pressure mode in the present experiments, allowing the upstream and downstream pressures (P_u and P_d) and mean pore fluid pressure ($P_f = \frac{(P_u+P_d)}{2}$) to be controlled within ± 0.049 MPa. The volume changes over time measured by ISCO pumps were taken as a measure of flow rate through the sample. A Lauda oil bath maintained at $42.0 \pm 0.1^\circ\text{C}$ was used to control the temperature of the ISCO pumps and gases flowing through the sample. A foam-polystyrene box was also constructed around the pressure vessel, syringe pumps, and oil bath to control the air temperature around the setup at $38.2 \pm 0.2^\circ\text{C}$, using an internal lamp, fan, and CAL 9900 PID-controller (cf. Hol and Spiers, 2012). The temperature was measured at the locations shown in **Figure 2** (T_{pt}) using PT-100 sensors with a resolution of 0.01°C . This all ensured the permeability tests were performed at $\sim 40^\circ\text{C}$. Note that, at employed boundary conditions, the term “(Terzaghi) effective stress” used in this study refers to Terzaghi effective confining pressure or Terzaghi effective normal stress, calculated as $P_c - P_f$.

Experimental Procedures

We performed one multi-stage experiment on the single cylindrical sample (**Figure 1**) at a constant temperature of 40°C . We measured permeability of the sample to helium, CH₄, and CO₂ under fixed volume versus stress boundary conditions, using the steady-state method, employing Terzaghi effective stresses of 14–41 MPa. The following stages were

conducted using helium, CH₄, helium, CO₂, and again helium (Stages I–V), in that order, as summarized in **Table 1**.

Stages I, III, V

Helium permeability. We measured helium permeability of the sample under the fixed stress boundary condition only because helium, as a non-sorbing gas, cannot induce coal swelling. In these stages, helium was first introduced into the sample at a given pore pressure and confining pressure. After stabilization, the flow-through test was then performed by increasing the upstream pressure by 0.4 MPa. The mean helium pressure employed in these stages was 3.2, 5.2, 7.2, and 9.2 MPa, respectively. At each mean fluid pressure, the confining pressure was stepped up (and down) in the range of 18–38 MPa, in an attempt to determine the effect of confining pressure on permeability and whether such effect is reversible. As a result, we obtained permeability of the sample to helium at Terzaghi effective stresses of 13–35 MPa for Stages I, III, V. Note that helium behaves as a supercritical fluid at PT conditions employed in this study.

Stage II

CH₄ permeability. We measured the CH₄ permeability of the sample under both fixed volume and fixed stress boundary conditions. The confining pressure was first applied, followed by closure of the valve F (see **Figure 2**). The initial confining pressure before the introduction of CH₄ under the fixed volume boundary condition was 25.4 MPa. CH₄ was then injected into the sample, and the pore pressure was controlled at 10 MPa using the downstream pump. Note that the P_c-P_f-T conditions thus achieved were similar to those at a burial depth of 1 km. After the introduction of CH₄, the confining pressure measured by the pressure transducer instantaneously increased due to poroelastic effects, followed by a gradual increase that reflected sorption-induced swelling. The confining pressure was finally increased to 38.8 MPa after 171 h. During the sorption-induced swelling process, the CH₄ uptake (mmol/g) was obtained from the volume change in the downstream pump, and permeability at given confining pressures was measured through flow-through tests performed by increasing the upstream pressure by 0.4 MPa. Note that each permeability test lasted for 20–40 min, and during such short intervals, the change in the total mass of two ISCO pumps was negligible. As equilibrium was approached with CH₄ at a pore fluid pressure of 10 MPa under the fixed volume boundary condition, we performed the permeability tests under the fixed stress boundary condition (i.e., the valve F was maintained open and the confining pressure was adjusted to remain constant using the hand pump), following similar procedures described in Stage I. By comparison, the mean fluid pressures of 10.2, 8.2, 6.2, and 3.2 MPa, and Terzaghi effective stresses of 14–34 MPa, were employed, respectively. Note that we waited several to tens of hours for re-equilibration after a change in either pore pressure or confining pressure, prior to each flow-through test performed under the fixed stress boundary condition.

Stage IV

CO₂ permeability. Following similar procedures as described in Stage II, we measured permeability of the sample to CO₂ under both the fixed volume and fixed stress boundary conditions. Under the fixed volume boundary condition, CO₂ was injected into the sample, using the downstream pump, at an initial confining pressure of ~25 MPa. Note that we could not measure CO₂ uptake properly during the injection because it is quite difficult to eliminate poroelastic effects, particularly when CO₂ pressure and confining pressure cannot be maintained constant. After CO₂ pressure stabilization at 10 MPa, we performed the flow-through test continuously, employing a pressure difference of ~2 MPa between upstream and downstream, achieved by increasing the upstream pressure. Note that this process was unlike the flow-through tests performed at intervals during CH₄ sorption, employing a pressure difference of ~0.4 MPa. The near equilibration took around ~44 h, and the confining pressure increased to 52 MPa. Also note that the steady-state method cannot properly give the adsorption capacity for CO₂ during the flow-through test in the permeability range of 10⁻¹⁸–10⁻¹⁹ m². Following the similar procedures performed for CH₄ and helium under the fixed stress condition, we performed the permeability tests at mean fluid pressures of 11, 13, 15 MPa, employing Terzaghi effective stresses of 14–29 MPa. The pressure difference between upstream and downstream was maintained at ~2 MPa during all flow-through tests using CO₂. Note that CO₂ behaves as a supercritical fluid at the conditions employed, so that the effects of phase change can be eliminated.

Note that, before each stage, the sample was evacuated for several days, using a vacuum pump, in an attempt to fully remove the residual gas from the sample used in the previous stage.

Data Acquisition and Processing

The system temperature, confining pressure signals were recorded using a computer equipped with LabView-based software, at a sampling rate of 0.2 Hz. Pump pressure and volume signals were recorded using ISCO 65D panel software at a sampling rate of 0.2 Hz. Note that the data obtained were processed by removing data intervals corresponding to pump re-stroking or other maintenance, correcting for both volume and time offsets accordingly.

Considering the evacuation process performed prior to the flow-through tests and the PT conditions employed in the present study, we focused on single-phase flow and neglected the influence of gas slippage (Klinkenberg) on permeability evolution (e.g., Peach, 1991). The obtained data were accordingly used to calculate the apparent Darcy permeability (κ_{app}) of the sample to helium, CH₄, and CO₂, corrected for the compressibility of the gas or supercritical fluid, using the following equation (e.g., Tanikawa and Shimamoto, 2009):

$$\kappa_{app} = \frac{2Q\eta L}{A} \frac{P_d}{P_u^2 - P_d^2}, \quad (1)$$

where $Q = \frac{Q_u + Q_d}{2}$ (m³ s⁻¹) represents the fluid flux traversing the sample, in which Q_u and Q_d are fluid fluxes measured at specific

times from the volume change of the upstream and downstream pump, respectively, versus time data using a moving average method, followed by linear regression over intervals up to 40 min; η is the dynamic viscosity of the fluid (Pa s), whose values for the fluids used at the employed PT conditions in this study were obtained from the open source of National Institute of Standards and Technology (NIST), i.e., <https://webbook.nist.gov/chemistry/fluid/>; A (m²) and L (m) represent the cross-sectional area and length of the sample, respectively; and P_u and P_d are the pump pressures (Pa) measured upstream and downstream, respectively. The pressure difference between upstream and downstream (i.e., $P_u - P_d$) was verified by the measurements of a differential pressure transducer. Note that, in this study, we determined the error bar of the permeability data points by using the absolute error method, obtained from the permeability values calculated from Q_u and Q_d . Also note that no or little leakage of the pumps was found to be negligible compared to the fluid flux traversing the sample.

RESULTS

Permeability of the sample to helium, CH₄, and CO₂ as a function of Terzaghi effective stress under the fixed stress boundary condition was obtained. Permeability evolution associated with development of the confining pressure was also obtained for the fixed volume boundary condition performed on CH₄ and CO₂. All data files obtained from the experiment can be found *via* the link <https://public.yoda.uu.nl/geo/UU01/XOJCFK.html>, and key data are illustrated in **Figures 3–5**.

Broadly speaking, the permeability of the coal sample measured at the Terzaghi effective stresses employed in this study (in the range of 14–41 MPa) lied in the range of 10⁻¹⁹–10⁻¹⁷ m², showing the order of permeability measured was helium > CH₄ > CO₂ at similar Terzaghi effective stresses. The permeability versus Terzaghi effective stress yielded a clear non-linear correlation, and the permeability reduced ~1–2 orders with increasing Terzaghi effective stress from 14 to 41 MPa. Note here that we, after the experiment, observed some new small visible fractures formed on the surface of the sample, but no mechanical failure (see **Figure 1**).

Helium Permeability

Permeability measured for helium at a fixed stress boundary condition, illustrated in **Figure 3**, yielded a function of Terzaghi effective stress, showing a near reversible process at Stages I and III, but clear hysteresis at Stage V. It is also found in **Figure 3** that the permeability obtained before and after CH₄ flow-through tests (Stages I, III), and after CO₂ flow-through tests, shows different values even at similar Terzaghi effective stresses, yielding an order of Stage I > Stage III > Stage V. Specifically, at Stage I, the permeability was 6.5 × 10⁻¹⁷ m² at a Terzaghi effective stress of 15 MPa and reduced to 6.5 × 10⁻¹⁸ m² at 35 MPa (**Figure 3A**). The permeability measured at Stage III was a little smaller than that measured at Stage I (**Figure 3B**). However, by comparison with the permeability obtained at Stages I and III, it reduced a factor of 3–6 at similar Terzaghi effective

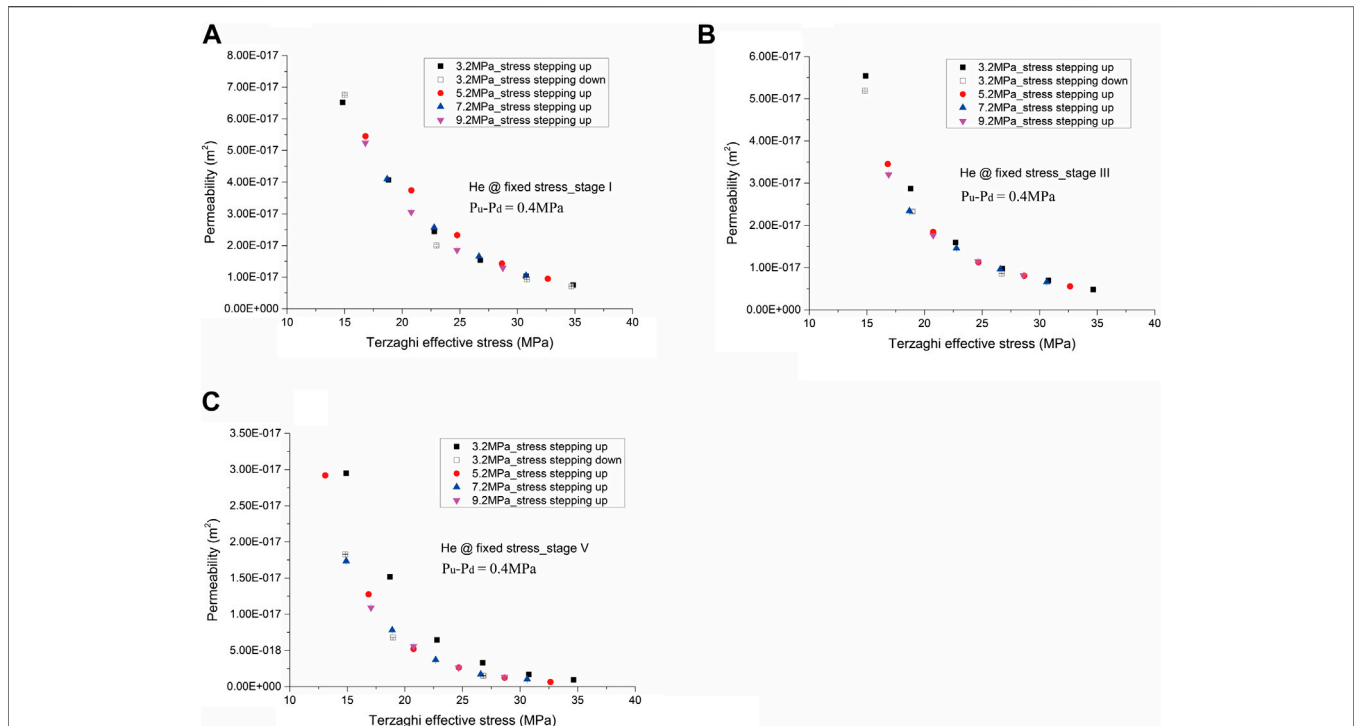


FIGURE 3 | Permeability of the sample to helium against Terzaghi effective stress performed under the fixed stress boundary condition at (A) Stage I, (B) Stage III, and (C) Stage V.

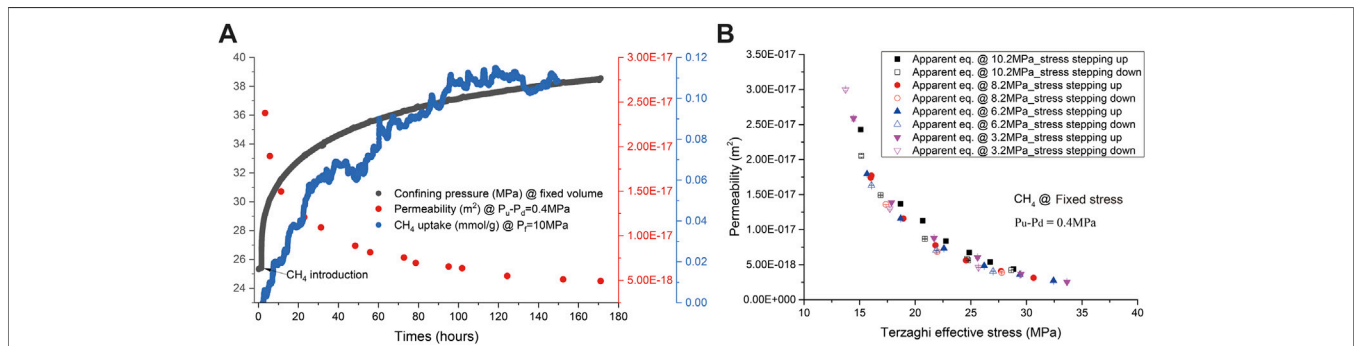


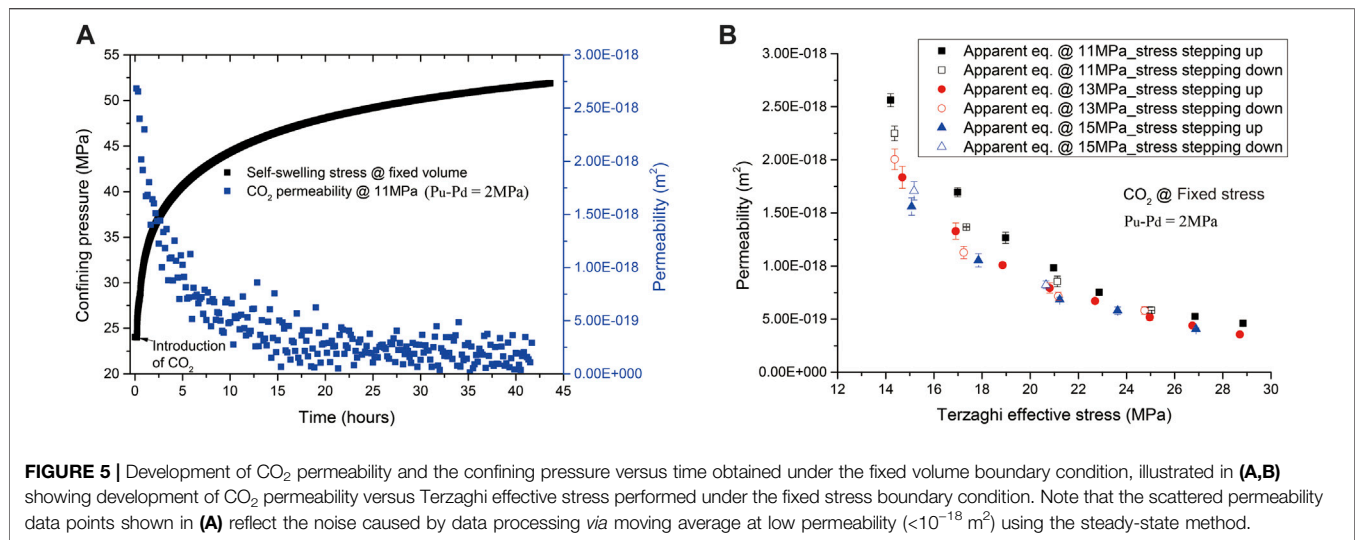
FIGURE 4 | Development of CH₄ permeability, the confining pressure, and CH₄ uptake against time obtained under the fixed volume boundary condition, illustrated in (A,B) showing development of CH₄ permeability as a function of Terzaghi effective stress performed under the fixed stress boundary condition.

stresses, after CO₂ flow-through tests, and behaved more sensitive to the change of Terzaghi effective stress. This indicates a permanent effect of CO₂ introduction on permeability evolution. In particular, the permeability measured at Stage V was $3 \times 10^{-17} m^2$ at 15 MPa and reduced to $9.5 \times 10^{-19} m^2$ at 35 MPa (Figure 3C).

CH₄ Permeability

The development of confining pressure and permeability of the sample associated with adsorption amounts during CH₄ flow-through tests performed under the fixed volume boundary condition is illustrated in Figure 4A. It is clearly seen that the confining pressure showed fast increase from 25.4 to ~28 MPa

within 1 h, followed by slow evolution up to 38.6 MPa until ~170 h with CH₄ uptake of ~0.11 mmol/g. The former may be dominated by an instant poroelastic effect and the latter by time-dependent sorption-induced swelling. In the meanwhile, the permeability reduced from $2.4 \times 10^{-17} m^2$ measured at a Terzaghi effective stress of ~19 MPa to $5 \times 10^{-18} m^2$ measured at ~28 MPa Terzaghi effective stress. The permeability of the sample measured under the fixed stress condition is shown in Figure 4B, as a function of Terzaghi effective stress. The permeability reduced from $3 \times 10^{-17} m^2$ measured at 14 MPa Terzaghi effective stress to $2.5 \times 10^{-18} m^2$ at 34 MPa, which are smaller, by a factor of 2, than those measured for helium at Stage I. This may suggest the effect of CH₄ sorption on permeability.



Also note that permeability versus Terzaghi effective stress plotted in **Figure 4B** showed little hysteresis, probably because the coal sample has been pre-treated with CH₄.

CO₂ Permeability

The development of confining pressure and permeability of the sample during CO₂ flow-through tests performed under the fixed volume boundary condition is plotted versus time in **Figure 5A**. The confining pressure showed fast increase from 24 to ~34 MPa in an hour, followed by a gradual change up to 52 MPa until ~44 h since first CO₂ introduction. This indicates the combined effects of poroelastic and sorption-induced swelling. Meanwhile, the permeability reduced from 2.7×10^{-18} m² obtained at a Terzaghi effective stress of ~14 MPa to 1.8×10^{-19} m² at ~52 MPa Terzaghi effective stress, which, in magnitude, are an order lower than those for CH₄ measured at similar Terzaghi effective stresses. Recall that we did not obtain the CO₂ uptake data in this flow-through test. The permeability of the sample measured under the fixed stress condition, plotted in **Figure 5B** against Terzaghi effective stress, showed that the permeability reduced from 2.6×10^{-18} m² measured at 14 MPa Terzaghi effective stress to 4×10^{-19} m² at 29 MPa. These also, in magnitude, are an order lower than those for CH₄ measured at similar Terzaghi effective stresses. Such a large difference in permeability may suggest, compared to CH₄, CO₂ has a faster sorption process, higher sorption-induced swelling, and a stronger sorption effect on permeability, which is consistent with the findings widely reported in the literature (e.g., Gensterblum et al., 2014). Also note that permeability versus Terzaghi effective stress plotted in **Figure 5B** showed hysteresis, suggesting a permanent change in transport paths of the sample.

Effect of Boundary Condition on Permeability: Fixed Volume Versus Fixed Stress

Permeability of the sample to CH₄ and CO₂ performed under fixed volume versus fixed stress boundary conditions, employing

the same pore fluid pressure, is plotted against Terzaghi effective stress in **Figure 6**. It is clear that permeability, even at similar Terzaghi effective stresses, measured under the fixed volume boundary condition is higher than that measured, at equilibration, under the fixed stress boundary condition, reflecting the effect of boundary condition on permeability. Interestingly, the lower the Terzaghi effective stress occurring at the initial sorption process under the fixed volume boundary condition, the higher the difference in permeability upon such effects. This may suggest the effect of boundary condition could be related to the degree of sorption equilibration, depending on diffusion. Particularly, for CH₄ shown in **Figure 6A**, permeability reduced by a factor up to ~2 at 18.4 MPa, while for CO₂ shown in **Figure 6B**, permeability reduced by an order at 25 MPa. This again reflects CO₂ has a stronger sorption effect on permeability evolution.

DISCUSSION

The flow-through experiment performed in this study demonstrated the permeability reduced exponentially with increasing effective stress, regardless of the fluids used as well as the boundary conditions employed. This suggests the permeability is stress-dependent. Importantly, our results also showed that, at similar Terzaghi effective stresses, the permeability of the sample to CO₂ is an order lower than that to CH₄, and the permeability to CH₄ is also 2–3 times lower than that to helium. This is in good agreement with experimental observations reported in the literature (e.g., Gensterblum et al., 2014). Moreover, our results shown in **Figure 6** demonstrated the effect of boundary condition on permeability. This all suggests sorption effects on permeability evolution, independently of poroelastic effects. Interestingly, the differences in helium permeability obtained in Stages I, III, and V suggest a permanent effect of sorption on permeability. It is difficult to distinguish, directly from the experiments, whether

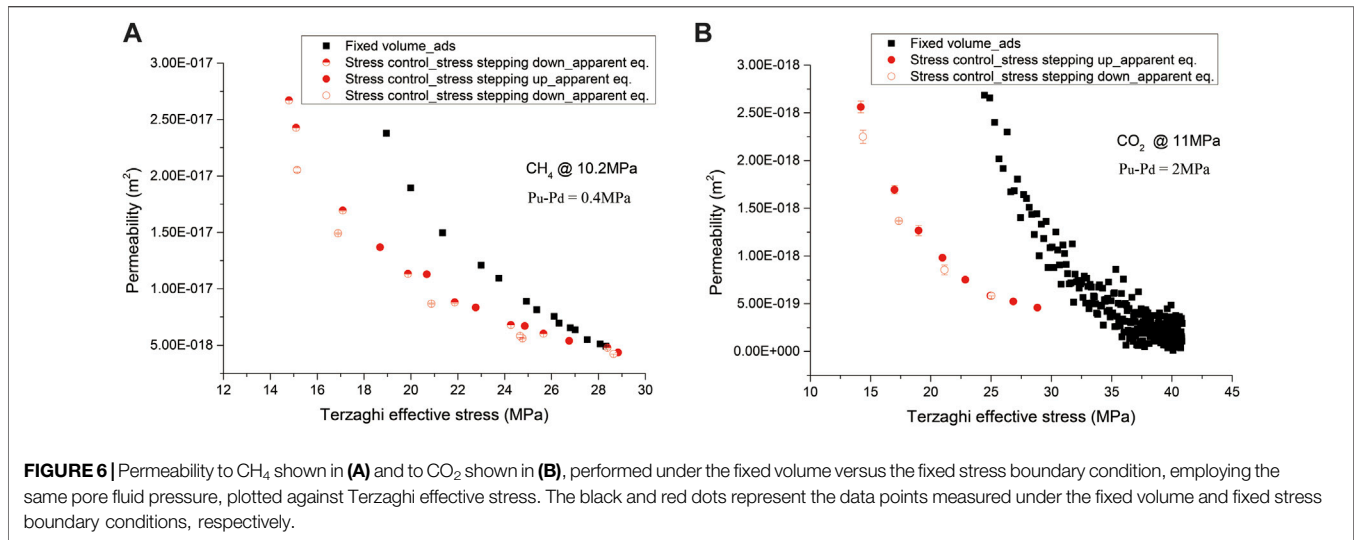


FIGURE 6 | Permeability to CH_4 shown in **(A)** and to CO_2 shown in **(B)**, performed under the fixed volume versus the fixed stress boundary condition, employing the same pore fluid pressure, plotted against Terzaghi effective stress. The black and red dots represent the data points measured under the fixed volume and fixed stress boundary conditions, respectively.

this permanent effect is caused by the change of effective stress or by adsorption, especially for the fixed volume boundary condition. Instead, we attempt to use a simple fracture permeability model proposed by Walsh (1981) for an elastic asperity loading framework (i.e., reversible deformation), to distinguish any permanent effects on permeability caused by diffusion-controlled adsorption/desorption. In the following, we will first investigate whether the Walsh permeability model can describe the direct effect of effective normal stress on permeability observed in this study. Subsequently, we will discuss the effects of sorption process on permeability and, finally, the implications of our findings for CO_2 -ECBM recovery.

Experimental Data Versus the Walsh Permeability Model: Effect of Normal Stress

Our results shown in Figure 3, Figure 4B, and Figure 5B demonstrate that the permeability of the coal sample containing visible fractures exponentially reduced with increasing Terzaghi effective stress. This is in good agreement with stress-dependent permeability of coal samples (Somerton et al., 1975; Durucan and Edwards, 1986; Gensterblum et al., 2014; Chen et al., 2011). We here quantitatively determine the direct correlation between permeability and effective stress, using the Walsh permeability model, in an attempt to capture the direct effect of effective normal stress on fracture permeability. Recall that the Walsh permeability model was constructed for describing the fracture permeability change between two roughness surfaces, with respect to the change in the applied effective stress, which considered the effect of elastic fracture asperity contacts on fracture permeability (κ). The model can be expressed as (Walsh, 1981)

$$\frac{\kappa}{\kappa_0} = \left[1 - a \ln \left(\frac{\sigma_e}{\sigma_{e0}} \right) \right]^3 \left[\frac{1 - b(\sigma_e - \sigma_{e0})}{1 + b(\sigma_e - \sigma_{e0})} \right]. \quad (2)$$

Here, $a = 2\sqrt{2} \left(\frac{h}{D_0} \right)$ reflects the physical properties of fracture, where h (m) represents the root mean square value of the height distribution of the fracture surface and D_0 (m) represents the mean fracture aperture at the reference effective stress σ_{e0} and permeability κ_0 , and b (MPa^{-1}) is assumed to be a constant for the Hertzian contact, representing that the contact area increases linearly with the effective stress. Assuming the asperity area is far smaller than the surface area, i.e., the ratio of the asperity area over the surface area $\alpha \approx 0$, Eq. 2 approximately reduces to

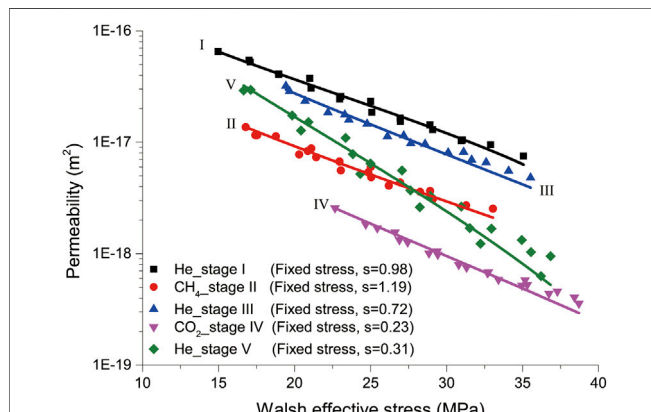
$$\frac{\kappa}{\kappa_0} = \left[1 - a \ln \left(\frac{\sigma_e}{\sigma_{e0}} \right) \right]^3. \quad (2a)$$

This simplification, in turn, is exactly in the same format as the cubic model using the exponential function expressing the correlation between the effective stress and the joint closure (cf. Cook, 1992). In addition, the effective stress is given by Walsh as $\sigma_e = P_c - sP_f$, where $s = 1 - \beta_s/\beta_f$ is identified as the “Walsh effective stress coefficient” in this study. β_s, β_f are the compressibility of the matrix and fracture, respectively. Note that the Walsh effective stress is assumed to exhibit the same deformation of the fracture as that acted by both the confining and fluid pressures. If $\beta_s \ll \beta_f$, s reduces to 1, equivalent to the Terzaghi effective stress, while if $\beta_s = \beta_f$, s reduces to 0.

We here focus on the permeability data obtained under the fixed stress boundary condition in which the coal sample was equilibrated with the gas/fluid at given P_c - P_f - T conditions. We further assumed that 1) the fracture contacts and roughness, i.e., the values of s , a , and b in Eq. 2, remained constant during the flow-through tests performed at each experimental stage (Stages I–V, see Table 1), while the values may be different between stages, implying permanent changes in coal structures and flow paths, and 2) the permeability development shown in Figure 3, Figure 4B, and Figure 5B for each stage is only dependent on the change in Walsh effective stress. Following the least square method and using the Walsh permeability model presented in Eq. 2, we obtained the parameters s , a , and b for each stage, as

TABLE 2 | List of the values of σ_{e0} and κ_0 used for each stage and parameter values obtained from the best fitting of Eq. 2 to the permeability data shown in Figure 7.

Parameter values	I	II	III	IV	V
s	0.98	1.19	0.72	0.23	0.31
a	0.07	0.52	0.58	0.67	0.75
b (MPa ⁻¹)	0.013	0.016	0.019	0.022	0.028
R^2	0.99	0.97	0.98	0.98	0.97
σ_{e0} (MPa)	14.97	16.79	19.68	22.66	17.11
κ_0 (m ²)	6.52×10^{-17}	1.37×10^{-17}	2.87×10^{-17}	2.56×10^{-18}	2.95×10^{-17}

**FIGURE 7** | Permeability measured at all stages performed under the fixed stress boundary condition, plotted in logarithms, as a function of the Walsh effective stress. Note that s is the Walsh effective stress coefficient, and the lines represent the best fittings of Eq. 2 to the data points. The values of σ_{e0} and κ_0 used for each stage and the parameter values obtained are listed in Table 2.

listed in Table 2. On this basis, the permeability data obtained for each stage are plotted in Figure 7, as a function of the Walsh effective stress. Note that the values of σ_{e0} and κ_0 used in each stage are also listed in Table 2. It is clearly seen from Figure 7 that the Walsh permeability model provides accurate descriptions of the permeability change caused by the change in effective normal stress ($R^2 \geq 0.97$), no matter which gases/fluids were used. Importantly, the parameter values listed in Table 2 lie in a reasonable range, properly reflecting the physical properties of the fracture, though the Walsh effective stress coefficient (s) obtained for CH₄ is more than unity. Although the value larger than 1 is inconsistent with the definition of the Walsh effective stress coefficient ($s = 1 - \beta_s/\beta_f$), it is also reported elsewhere that the Biot effective stress coefficient may be higher than 1 for deformation of sorbing media, probably due to sorption-induced swelling (Liu and Harpalani, 2014; Sang et al., 2017). This will be further discussed in *Effects of Sorption-Induced Swelling on Walsh Effective Stress Coefficient*.

Following the above assumptions, the difference in these parameter values obtained from helium permeability data measured at different stages may imply the permanent changes in fracture structure and transport paths upon the sorption effects. Note that the permeability to helium measured at Stage V was most sensitive to the Walsh

effective stress. This can be explained by the highest b value obtained at Stage V, as it means the contact areas of the fracture, after CO₂ adsorption, would increase the most, i.e., the aperture spacing would reduce the most, at given changes in the Walsh effective stress. This all indicates that the Walsh permeability model can well describe stress-dependent permeability of coal with respect to sorbing gases, given proper parameter values reflecting the sorption effects on fracture properties.

Effects of Stress–Strain–Sorption on Permeability Evolution

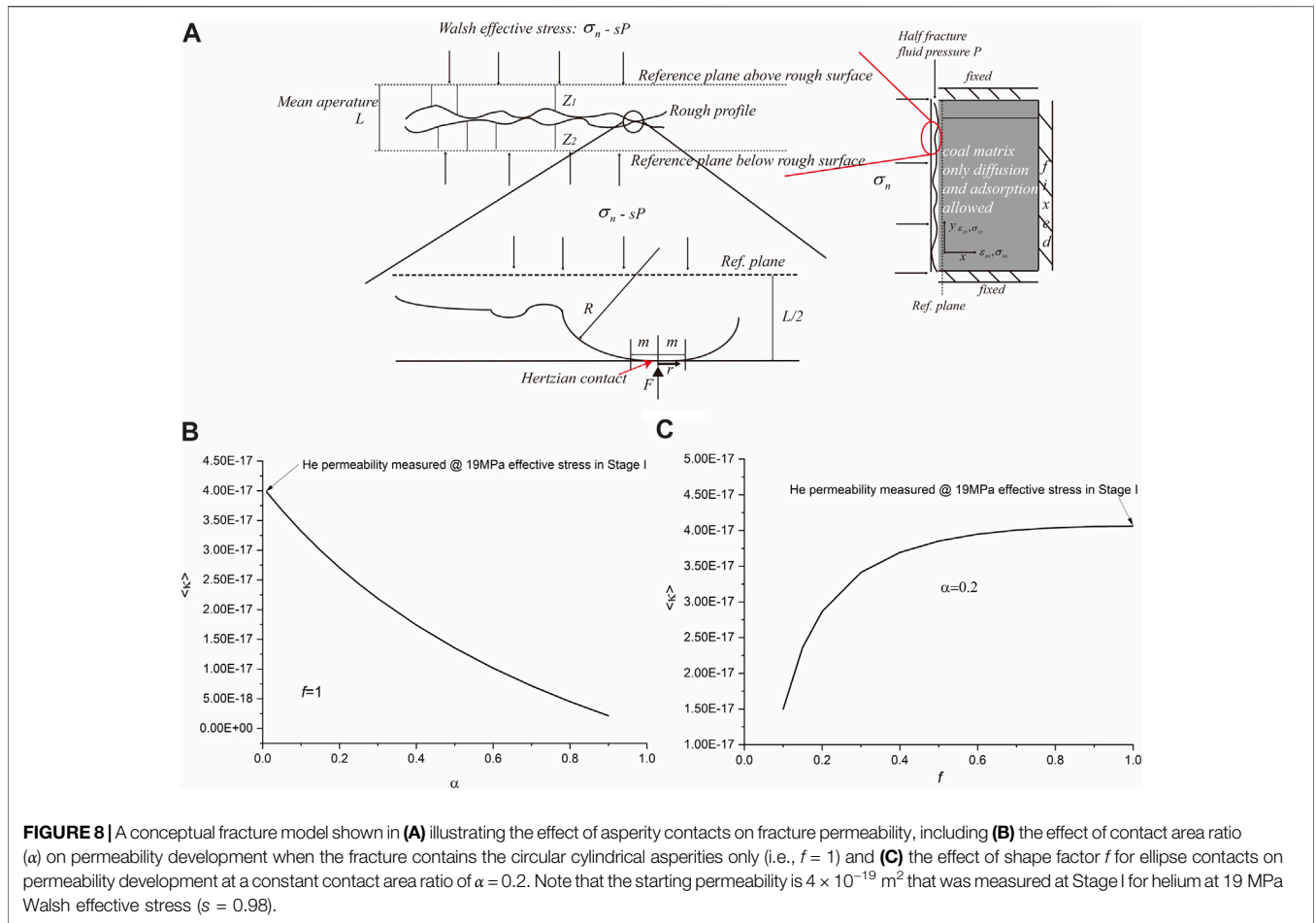
Apart from the stress-dependent permeability, Figure 7 also clearly indicates that permeability of the sample measured at similar Walsh effective stresses lies in the following order: κ for helium measured in Stages I and III $> \kappa_{CH_4} >> \kappa_{CO_2}$. This demonstrates the effects of sorption process on permeability. In this section, we first crudely investigate whether the largest difference in permeability observed between Stages I and IV can be explained by the change in contact areas of the fracture. We then attempt to explain the changes in Walsh effective stress coefficient observed between stages. Finally, we discuss the effects of sorption equilibration degree on permeability evolution under the fixed volume boundary condition.

Effective Permeability: Effect of Stress–Strain–Sorption Behavior on Fracture Contacts

Recall that the Walsh permeability model was used to determine how permeability changes with respect to the change in effective stress. This means that the large reduction in permeability upon CO₂ adsorption observed at similar Walsh effective stresses cannot be explained by the changes in parameter values listed in Table 2. In an attempt to gain insights into such sorption-induced permeability changes, we introduce the effective permeability $\langle \kappa \rangle$ of the fracture roughness illustrated in Figure 8A (Walsh, 1981). Walsh (1981), analog to the heat flow, proposed $\langle \kappa \rangle$ that has permeability κ of the smooth fracture containing the circular cylindrical asperities with the contact area ratio α , given as

$$\langle \kappa \rangle = \frac{1 - \alpha}{1 + \alpha} \kappa. \quad (3)$$

Zimmerman et al. (1992) modified the above relation for the ellipse contacts by introducing the shape factor f , as

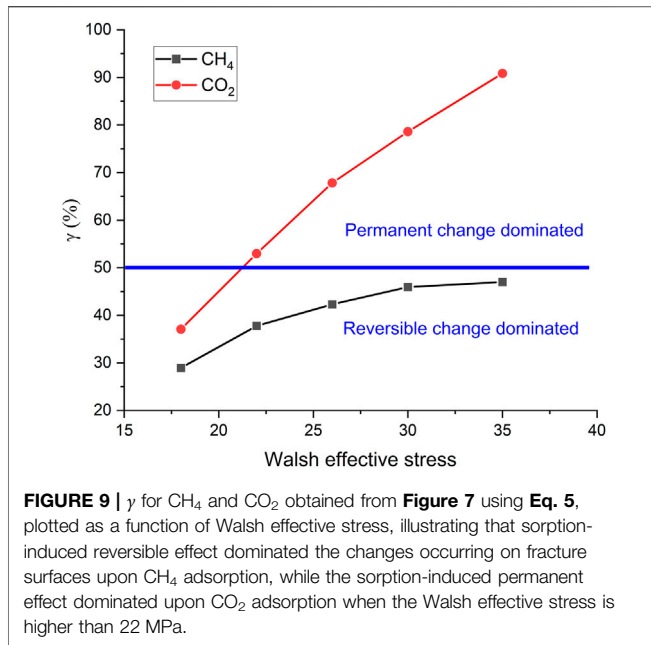


$$\langle \kappa \rangle = \frac{1 - f\alpha}{1 + f\alpha} \kappa, \tag{4}$$

where $f = \frac{(1+c)^2}{4c}$ and c is defined as the ratio of the minor to the major axis. It is clearly seen that Eq. 4 will reduce to Eq. 3, if $f = 1$.

Crude analysis performed using Eqs 3, 4 suggests the combined changes in contact area ratio and contact shape could reduce permeability from 4×10^{-17} to 4×10^{-18} or even lower (see Figures 8B,C), which is in good agreement with the change observed in Figure 7. This means the large reduction in permeability upon CO₂ adsorption may be explained by the changes in contact area and contact shape. Similar changes that occurred in the fracture structure caused by sorption-induced heterogeneous swelling are also reported by Wu et al. (2011). Such changes can be caused by the coupled stress-strain-sorption behavior of coal upon adsorption of CH₄ and CO₂ (Liu et al., 2016). Liu et al. (2016) constructed a thermodynamic model for describing adsorbed concentration of any sorbing gas/fluid by the coal matrix subjected to the applied stress states. The model demonstrates the higher the applied stress, the lower the adsorbed concentration. Considering the fracture structure illustrated in Figure 8A, the asperity solid contact with high normal stress would adsorb little CH₄ or

CO₂ accompanied by little sorption-induced swelling, while the free surfaces of the aperture having low normal stress would adsorb more CH₄ or CO₂, accompanied by large swelling. Such heterogeneous deformation occurring at fracture surfaces upon adsorption would lead to an increase in α and a reduction in f , accordingly reducing permeability. Note that such effects should be reversible, supported by the fact that the helium permeability measured after the sorption process is much higher than κ_{CH_4} and κ_{CO_2} measured at similar Walsh effective stresses. However, the difference in helium permeability obtained before and after CH₄ and CO₂ adsorption suggests a permanent change occurring on fracture surfaces. Such permanent changes may be caused by the heterogeneous deformation-induced microcracking mechanism during the coupled stress-strain-sorption process (Hol et al., 2012b). This is also consistent with the hysteresis observed in plots for permeability versus Terzaghi effective stress shown in Figures 4B, 5B. In addition, such permanent changes in fracture structure that occurred during the stress-strain-sorption process could be one of the mechanisms responsible for the change in parameters of s , a , and b (see Table 2). In addition, the chemical interaction between coal and supercritical CO₂ may also have some influence on the permanent changes of fracture structure and accordingly



on the permanent changes in permeability (Zhang et al., 2013; Chen et al., 2017).

To quantitatively evaluate the role of such permanent changes occurring on fracture surfaces in controlling permeability, we introduce a ratio γ expressing the relative change in permeability with respect to the helium permeability measured before the sorption process, defined as

$$\gamma = \frac{\Delta\kappa_{\text{helium}}}{\kappa_{\text{helium}} - \kappa_s} \times 100\%, \quad (5)$$

where $\Delta\kappa_{\text{helium}}$ represents the change in helium permeability measured at similar Walsh effective stresses before and after the sorption process and the term $(\kappa_{\text{helium}} - \kappa_s)$ represents the difference between permeability to helium measured after the sorption process and to the sorbing gas measured at a similar Walsh effective stress. It suggests such sorption-induced permanent changes dominated the permeability evolution if $\gamma > 50\%$; otherwise, the sorption-induced reversible changes dominated. γ for CH₄ and CO₂ obtained from Figure 7 using Eq. 5 is plotted against Walsh effective stress in Figure 9, reflecting the combined effects of reversible and permanent processes on sorption-induced permeability evolution. Particularly, CH₄ adsorption-induced changes that occurred on fracture surfaces were dominated by the reversible stress-strain-sorption effect, while CO₂ adsorption-induced changes were dominated by the permanent effect under conditions employed in this study (Walsh effective stress >22 MPa). Note this permanent change upon supercritical CO₂ may also be related to chemical extraction effects (Zhang et al., 2013; Chen et al., 2017).

Effects of Sorption-Induced Swelling on Walsh Effective Stress Coefficient

Figure 7 and Table 2 indicate that s experienced an increase from 0.98 to 1.19 upon CH₄ sorption, followed by a significant

reduction to ~ 0.3 upon CO₂ sorption. To explain such changes, we introduce a revised Walsh effective stress coefficient (s^a). Liu and Harpalani (2014) and Sang et al. (2017) revised the Biot effective stress coefficient by introducing an additional term considering the effect of sorption-induced swelling. By analogy with the expression given by them, the Walsh effective stress coefficient might be revised in a simple form as

$$s^a = 1 - \beta_s/\beta_f + K\varepsilon_v^{ads}/K_a, \quad (6)$$

where ε_v^{ads} represents adsorption-induced volumetric swelling strain, which is a function of σ -P-T (cf. Liu et al., 2016), and K represents the bulk modulus of the sample, while K_a represents the apparent bulk modulus measured using sorbing gas depending on ε_v^{ads} (cf. Hol et al., 2011; Hol et al., 2014). It is clear that the change in s^a should be determined by the competition between the change in compressibility β_s/β_f and the term $K\varepsilon_v^{ads}/K_a$, and it can be greater than 1.

Returning now to our data, the increase of s^a to 1.19 upon CH₄ adsorption suggests sorption-induced swelling dominated over the change in β_s/β_f . Note that s^a obtained from helium permeability data measured after CH₄ adsorption reduced from 0.98 to 0.72. This suggests the value for β_s/β_f also increased upon CH₄ adsorption/desorption. It is reasonable that such a change in β_s/β_f may be attributed to the formation of microfractures during the sorption process (Walsh, 1965; Zimmerman, 1985). Considering the coal sample was pre-treated with CH₄ to the confining pressure of 30.7 MPa, compared to heterogeneous swelling effects, the sorption-induced swelling stress up to 38.8 MPa upon CH₄ adsorption under the fixed volume boundary condition may dominate. Note that the change in β_s/β_f upon CH₄ desorption and evacuation cannot be completely eliminated (Espinoza et al., 2015). By contrast, $s^a = 0.23$ suggests, upon CO₂ adsorption, the change in β_s/β_f dominates. Assuming similar values of $K\varepsilon_v^{ads}/K_a$ obtained for CH₄ and CO₂, the change in β_s/β_f caused by CO₂ adsorption-induced swelling is much larger. In other words, after CO₂ adsorption, the compressibility of coal matrix is much closer to fracture compressibility. This is consistent with the fact that the swelling stress caused by CO₂ adsorption-induced swelling under the fixed volume boundary condition was ~ 52 MPa, which is much higher than that caused by CH₄ adsorption. This is also supported by Hol et al. (2012b) who observed the formation of new microfractures of the Brezesczce coal matrix during the first exposure to CO₂ under unconfined boundary conditions. In addition, s^a obtained from helium flow-through tests performed at Stage V was still 0.31, suggesting a permanent change in coal structure upon CO₂ sorption. This is also in good agreement with the larger hysteresis behavior of permeability versus Terzaghi effective stress observed for CO₂, as well as the mechanisms discussed in *Effective Permeability: Effect of Stress-Strain-Sorption Behavior on Fracture Contacts* that sorption-induced permanent changes dominated at the Walsh effective stresses employed in this study for CO₂.

Now, we discuss the term $K\varepsilon_v^{ads}/K_a$. Our previous studies on the Brezesczce coal showed the volumetric swelling strain (ε_v^{ads}),

TABLE 3 | List of the values of σ_{e0} and κ_0 used for fitting and parameter values obtained from the best fitting of Eq. 2 to the permeability data shown in Figure 10.

Parameter values		s	a	b (MPa ⁻¹)	R ²	σ_{e0} (MPa)	κ_0 (m ²)
CH ₄	Fixed stress	1.19	0.52	0.016	0.97	16.79	1.37×10^{-17}
	Fixed volume	1.20	0.68	0.026	0.99	16.91	2.38×10^{-17}
CO ₂	Fixed stress	0.23	0.67	0.022	0.98	22.66	2.56×10^{-18}
	Fixed volume	0.85	0.74	0.037	0.98	26.07	2.68×10^{-18}

at equilibrium, was 1.29–1.39% due to CH₄ adsorption at a confining pressure of 11 MPa and 10 MPa CH₄ pressure (Liu et al., 2016) and was 1.83% to CO₂ adsorption at a confining pressure of 16 and 15 MPa CO₂ pressure (Hol et al., 2012), respectively. Combining the values of s^a and ϵ_v^{ads} obtained for CH₄ and CO₂, together with the term $K\epsilon_v^{ads}/K_a$, it remains acceptable that, upon adsorption of CH₄ or CO₂, the ratio of K/K_a might be ~10 at the conditions employed in this study (Hol et al., 2011; Hol et al., 2014).

Effect of Sorption Equilibration Degree on Permeability

Permeability against Terzaghi effective stress shown in Figure 6 suggests an apparent effect of boundary condition on permeability at similar Terzaghi effective stresses. Corrected for such effect on parameters s , a , and b (see Table 3), permeability plotted in Figure 10 as a function of Walsh effective stress demonstrates the similar results that permeability measured under the fixed volume boundary condition is higher than that measured at similar Walsh effective stresses under the fixed stress boundary condition that was equilibrated with CH₄/CO₂ and that the largest difference occurred at the initial sorption process. This suggests that gradual, diffusion-controlled equilibration also plays a role in changing the fracture structure through the mechanism discussed in *Effective Permeability: Effect of Stress–Strain–Sorption Behavior on Fracture Contacts*, as illustrated in Figure 8 (Liu et al., 2017; Wang et al., 2021). This is also supported by the evidence that CH₄ uptake by the Brezesczce coal obtained from this study performed under the fixed volume boundary condition was 0.11 mmol/g, which is ~7 times lower than that obtained, at equilibrium, from our previous study performed, at similar P_c – P_f – T conditions, under the fixed stress boundary condition (Liu et al., 2016). In addition, this mechanism, together with the mechanisms discussed in *Effects of Sorption-Induced Swelling on Walsh Effective Stress Coefficient*, could also explain why the values for the Walsh effective stress coefficient obtained under the fixed volume boundary condition are higher than those obtained under the fixed stress boundary condition. Similarly, Liu and co-authors (Liu et al., 2011c; Peng et al., 2014) proposed that diffusion-controlled time-dependent sorption-induced swelling as a mechanism caused permeability of coal to CO₂ and CH₄ showing a “V” shape with increasing pore fluid pressure at a fixed confining pressure that was observed by Wang et al. (2011).

Implications for ECBM and Reservoir Modeling

The results obtained from our flow-through experiment, performed at 40°C under the fixed volume boundary condition,

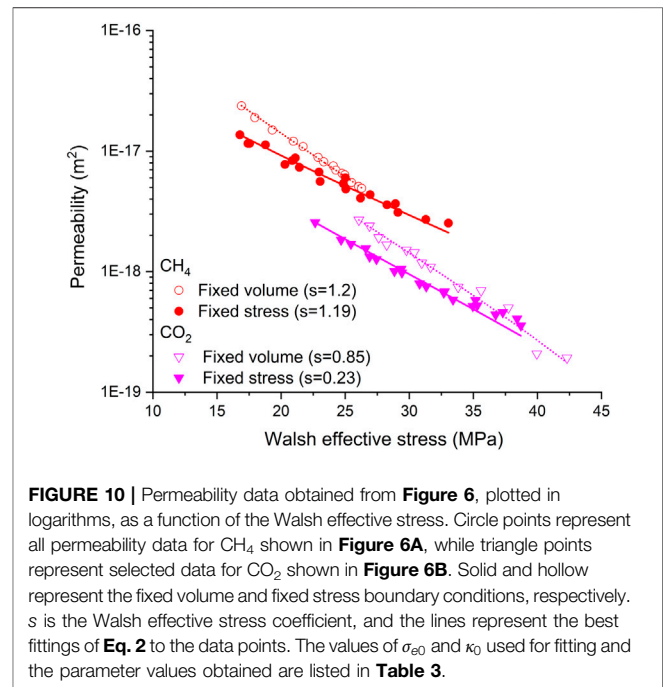


FIGURE 10 | Permeability data obtained from Figure 6, plotted in logarithms, as a function of the Walsh effective stress. Circle points represent all permeability data for CH₄ shown in Figure 6A, while triangle points represent selected data for CO₂ shown in Figure 6B. Solid and hollow represent the fixed volume and fixed stress boundary conditions, respectively. s is the Walsh effective stress coefficient, and the lines represent the best fittings of Eq. 2 to the data points. The values of σ_{e0} and κ_0 used for fitting and the parameter values obtained are listed in Table 3.

employing an initial confining pressure of ~25 MPa and 10 MPa pore fluid pressure, imply that injecting CO₂ into coal seams at a burial depth of ~1 km with initial permeability in the order of 10^{-17} would result in a dramatical reduction in permeability by ~2 orders, accompanied by permanent changes occurring in transport paths. This, together with our results obtained under the fixed stress boundary condition, further demonstrates that permeability evolution of coal seam during CO₂-ECBM recovery operating at *in situ* conditions could be strongly influenced by the fully coupled stress–strain–sorption–diffusion effects, involving 1) self-stress generated by time-dependent adsorption-induced swelling or desorption-induced shrinkage plus instant poroelastic effects, 2) the change in (Walsh) effective stress coefficient upon sorption-induced swelling, 3) sorption-induced closure of transport paths independently of poroelastic effect, and 4) diffusion-controlled heterogeneous gas penetration and equilibration. This may offer a new basis to enhance coal seam permeability by controlling those mechanisms.

Regarding reservoir modeling, our analysis suggests the Walsh permeability model offers a promising basis for relating permeability evolution to the change of *in situ* stress, regardless of boundary conditions, using appropriate parameter values corrected for the effects of

stress–strain–sorption. The parameter values can be obtained from the lab experiments, but it remains unclear whether those values can be extrapolated to the field predictions. Importantly, our results strongly suggest monitoring evolution of *in situ* stresses during CO₂-ECBM recovery may offer the most promising basis for predicting reservoir permeability evolution.

CONCLUSION

In this study, we investigated the coupled stress–strain–sorption effects on coal permeability evolution under the fixed volume versus the fixed stress boundary conditions, by performing flow-through tests on a cylindrical bituminous coal sample with respect to helium, CH₄, and CO₂, employing PT conditions equivalent to a burial depth of ~1 km. Using the framework of the elastic asperity loading model developed by Walsh as a reference model, we determined the specific mechanisms responsible for permeability evolution upon sorption process, both qualitatively and quantitatively. The main findings are summarized as follows:

- 1) The Brezeczko coal sample used in this study shows helium permeability, at a constant Terzaghi effective stress of 15 MPa, which decreases from $6.5 \times 10^{-17} \text{ m}^2$ measured before CH₄ introduction, to $5.5 \times 10^{-17} \text{ m}^2$ after CH₄ sorption, and to $1.7\text{--}3 \times 10^{-17} \text{ m}^2$ after CO₂ sorption, demonstrating a permanent change upon sorption.
- 2) Regardless of the boundary conditions employed and the fluids used in this study, the permeability of the coal sample decreased exponentially with increasing Terzaghi effective stress, in a manner that can be described by the Walsh permeability model. This finding offers a promising basis for predicting permeability evolution with respect to *in situ* stress changes, i.e., using the Walsh permeability model with appropriate parameter values corrected for the stress–strain–sorption effects.
- 3) Permeability obtained at similar Walsh effective stresses showed $\kappa_{\text{helium}} > \kappa_{\text{CH}_4} \gg \kappa_{\text{CO}_2}$, no matter whether performed under the fixed stress or the fixed volume boundary condition. This demonstrates that CO₂ exerts the strongest sorption effects on permeability evolution.
- 4) Permeability measured under the fixed volume boundary condition, particularly at the initial sorption process, was higher than that measured at equilibration under the fixed stress boundary condition, even at similar Walsh effective

stresses. This apparent effect indicates diffusion-controlled equilibration also plays a considerable role in permeability evolution occurring at a constant Walsh effective stress.

- 5) Permeability evolution of coal seams with respect to CH₄ or CO₂ at *in situ* PT and boundary conditions can be expected to be strongly influenced by the coupled effects of a) self-stress development induced by sorption-induced swelling, b) the change in (Walsh) effective stress coefficient upon sorption-induced swelling, c) sorption-induced closure of transport paths independently of poroelastic effects, and d) heterogeneous gas penetration and equilibration, caused by slow diffusion.

DATA AVAILABILITY STATEMENT

The original data package of this research has been published on EPOS Reposit, and can be found via the link <https://public.yoda.uu.nl/geo/UU01/XOJCFK.html>.

AUTHOR CONTRIBUTIONS

All the authors performed investigation and research. Specifically, JL performed experiments, processed data, and wrote the original draft under the supervision of CS. JL and CS formulated the ideas and research goals of this paper. CS conducted a critical review and revision.

FUNDING

The China Scholarship Council (CSC) is thanked for financial support to the first author to perform this experimental research. The National Natural Science Foundation of China (NSFC; project No. 41802230) and the Natural Science Foundation of Guangzhou City (project No. 202002030144) are also appreciated for their support to the first author to finish/publish this paper.

ACKNOWLEDGMENTS

The experimental research was conducted at HPT Lab. Eimert de Graaff, Gert Kastelein, and Floris van Oort are thanked for their technical support. Vincent Brunst is thanked for his technical support to publish the original data package on EPOS Repository.

REFERENCES

- Brown, S. R., and Scholz, C. H. (1985). Closure of Random Elastic Surfaces in Contact. *J. Geophys. Res.* 90, 5531–5545. doi:10.1029/jb090ib07p05531
- Brown, S. R., and Scholz, C. H. (1986). Closure of Rock Joints. *J. Geophys. Res.* 91, 4939. doi:10.1029/jb091ib05p04939
- Chen, R., Qin, Y., Wei, C., Wang, L., Wang, Y., and Zhang, P. (2017). Changes in Pore Structure of Coal Associated with Sc-CO₂ Extraction during CO₂-ECBM. *Appl. Sci.* 7, 931. doi:10.3390/app7090931
- Chen, Z., Liu, J., Pan, Z., Connell, L. D., and Elsworth, D. (2012). Influence of the Effective Stress Coefficient and Sorption-Induced Strain on the Evolution of Coal Permeability: Model Development and Analysis. *Int. J. Greenhouse Gas Control.* 8, 101–110. doi:10.1016/j.ijggc.2012.01.015
- Chen, Z., Pan, Z., Liu, J., Connell, L. D., and Elsworth, D. (2011). Effect of the Effective Stress Coefficient and Sorption-Induced Strain on the Evolution of Coal Permeability: Experimental Observations. *Int. J. Greenhouse Gas Control.* 5, 1284–1293. doi:10.1016/j.ijggc.2011.07.005
- Cook, N. G. W. (1992). Natural Joints in Rock: Mechanical, Hydraulic and Seismic Behaviour and Properties under normal Stress. *Int. J. Rock Mech. Mining Sci. Geomechanics Abstr.* 29, 198–223. doi:10.1016/0148-9062(92)93656-5

- Day, S., Fry, R., and Sakurovs, R. (2012). Swelling of Coal in Carbon Dioxide, Methane and Their Mixtures. *Int. J. Coal Geology*, 93, 40–48. doi:10.1016/j.coal.2012.01.008
- Durucan, S., and Edwards, J. S. (1986). The Effects of Stress and Fracturing on Permeability of Coal. *Mining Sci. Technology* 3 (3), 205–216. doi:10.1016/s0167-9031(86)90357-9
- Espinoza, D. N., Pereira, J.-M., Vandamme, M., Dangla, P., and Vidal-Gilbert, S. (2015). Desorption-induced Shear Failure of Coal Bed Seams during Gas Depletion. *Int. J. Coal Geology*, 137, 142–151. doi:10.1016/j.coal.2014.10.016
- Espinoza, D. N., Vandamme, M., Dangla, P., Pereira, J.-M., and Vidal-Gilbert, S. (2016). Adsorptive-mechanical Properties of Reconstituted Granular Coal: Experimental Characterization and Poromechanical Modeling. *Int. J. Coal Geology*, 162, 158–168. doi:10.1016/j.coal.2016.06.003
- Espinoza, D. N., Vandamme, M., Pereira, J.-M., Dangla, P., and Vidal-Gilbert, S. (2014). Measurement and Modeling of Adsorptive-Poromechanical Properties of Bituminous Coal Cores Exposed to CO₂: Adsorption, Swelling Strains, Swelling Stresses and Impact on Fracture Permeability. *Int. J. Coal Geology*, 134–135, 80–95. doi:10.1016/j.coal.2014.09.010
- Fujioka, M., Yamaguchi, S., and Nako, M. (2010). CO₂-ECBM Field Tests in the Ishikari Coal Basin of Japan. *Int. J. Coal Geology*, 82, 287–298. doi:10.1016/j.coal.2010.01.004
- Gensterblum, Y., Ghanizadeh, A., and Krooss, B. M. (2014). Gas Permeability Measurements on Australian Subbituminous Coals: Fluid Dynamic and Poroelastic Aspects. *J. Nat. Gas Sci. Eng.* 19, 202–214. doi:10.1016/j.jngse.2014.04.016
- Hol, S., Gensterblum, Y., and Massarotto, P. (2014). Sorption and Changes in Bulk Modulus of Coal - Experimental Evidence and Governing Mechanisms for CBM and ECBM Applications. *Int. J. Coal Geology*, 128–129, 119–133. doi:10.1016/j.coal.2014.04.010
- Hol, S., Peach, C. J., and Spiers, C. J. (2011). Applied Stress Reduces the CO₂ Sorption Capacity of Coal. *Int. J. Coal Geology*, 85, 128–142. doi:10.1016/j.coal.2010.10.010
- Hol, S., Peach, C. J., and Spiers, C. J. (2012a). Effect of 3-D Stress State on Adsorption of CO₂ by Coal. *Int. J. Coal Geology*, 93, 1–15. doi:10.1016/j.coal.2012.01.001
- Hol, S., and Spiers, C. J. (2012). Competition between Adsorption-Induced Swelling and Elastic Compression of Coal at CO₂ Pressures up to 100MPa. *J. Mech. Phys. Sol.* 60 (11), 1862–1882. doi:10.1016/j.jmps.2012.06.012
- Hol, S., Spiers, C. J., and Peach, C. J. (2012b). Microfracturing of Coal Due to Interaction with CO₂ under Unconfined Conditions. *Fuel* 97, 569–584. doi:10.1016/j.fuel.2012.02.030
- Karacan, C. Ö. (2003). Heterogeneous Sorption and Swelling in a Confined and Stressed Coal during CO₂ Injection. *Energy Fuels* 17 (6), 1595–1608. doi:10.1021/ef0301349
- Karacan, C. Ö. (2007). Swelling-induced Volumetric Strains Internal to a Stressed Coal Associated with CO₂ Sorption. *Int. J. Coal Geology*, 72, 209–220. doi:10.1016/j.coal.2007.01.003
- Kiyama, T., Nishimoto, S., Fujioka, M., Xue, Z., Ishijima, Y., Pan, Z., et al. (2011). Coal Swelling Strain and Permeability Change with Injecting Liquid/supercritical CO₂ and N₂ at Stress-Constrained Conditions. *Int. J. Coal Geology*, 85, 56–64. doi:10.1016/j.coal.2010.09.010
- Laubach, S. E., Marrett, R. A., Olson, J. E., and Scott, A. R. (1998). Characteristics and Origins of Coal Cleat: A Review. *Int. J. Coal Geology*, 35, 175–207. doi:10.1016/s0166-5162(97)00012-8
- Levine, J. R. (1996). Model Study of the Influence of Matrix Shrinkage on Absolute Permeability of Coal Bed Reservoirs. *Geol. Soc. Lond. Spec. Publ.* 109, 197–212. doi:10.1144/gsl.sp.1996.109.01.14
- Liu, J., Chen, Z., Elsworth, D., Miao, X., and Mao, X. (2011a). Evolution of Coal Permeability from Stress-Controlled to Displacement-Controlled Swelling Conditions. *Fuel* 90, 2987–2997. doi:10.1016/j.fuel.2011.04.032
- Liu, J., Chen, Z., Elsworth, D., Qu, H., and Chen, D. (2011b). Interactions of Multiple Processes during CBM Extraction: A Critical Review. *Int. J. Coal Geology*, 87, 175–189. doi:10.1016/j.coal.2011.06.004
- Liu, J., Fokker, P. A., and Spiers, C. J. (2017). Coupling of Swelling, Internal Stress Evolution, and Diffusion in Coal Matrix Material during Exposure to Methane. *J. Geophys. Res. Solid Earth* 122 (2), 844–865. doi:10.1002/2016jb013322
- Liu, J., Spiers, C. J., Peach, C. J., and Vidal-Gilbert, S. (2016). Effect of Lithostatic Stress on Methane Sorption by Coal: Theory vs. experiment and Implications for Predicting *In-Situ* Coalbed Methane Content. *Int. J. Coal Geology*, 167, 48–64. doi:10.1016/j.coal.2016.07.012
- Liu, J., Wang, J., Chen, Z., Wang, S., Elsworth, D., and Jiang, Y. (2011c). Impact of Transition from Local Swelling to Macro Swelling on the Evolution of Coal Permeability. *Int. J. Coal Geology*, 88, 31–40. doi:10.1016/j.coal.2011.07.008
- Liu, S., and Harpalani, S. (2014). Determination of the Effective Stress Law for Deformation in Coalbed Methane Reservoirs. *Rock Mech. Rock Eng.* 47, 1809–1820. doi:10.1007/s00603-013-0492-6
- Moore, T. A. (2012). Coalbed Methane: A Review. *Int. J. Coal Geology*, 101, 36–81. doi:10.1016/j.coal.2012.05.011
- Palmer, I. (2009). Permeability Changes in Coal: Analytical Modeling. *Int. J. Coal Geology*, 77, 119–126. doi:10.1016/j.coal.2008.09.006
- Pan, Z., and Connell, L. D. (2007). A Theoretical Model for Gas Adsorption-Induced Coal Swelling. *Int. J. Coal Geology*, 69, 243–252. doi:10.1016/j.coal.2006.04.006
- Pan, Z., and Connell, L. D. (2012). Modelling Permeability for Coal Reservoirs: A Review of Analytical Models and Testing Data. *Int. J. Coal Geology*, 92, 1–44. doi:10.1016/j.coal.2011.12.009
- Peach, C. J. (1991). Influence of Deformation on the Fluid Transport Properties of Salt Rocks. *Geologica Ultraiectina* 77, 1–238. (PhD thesis).
- Peng, Y., Liu, J., Wei, M., Pan, Z., and Connell, L. D. (2014). Why Coal Permeability Changes under Free Swellings: New Insights. *Int. J. Coal Geology*, 133, 35–46. doi:10.1016/j.coal.2014.08.011
- Pini, R., Ottiger, S., Burlini, L., Storti, G., and Mazzotti, M. (2009). Role of Adsorption and Swelling on the Dynamics of Gas Injection in Coal. *J. Geophys. Res.* 114, B04203. doi:10.1029/2008jb005961
- Pone, J. D. N., Halleck, P. M., and Mathews, J. P. (2009). Sorption Capacity and Sorption Kinetic Measurements of CO₂ and CH₄ in Confined and Unconfined Bituminous Coal. *Energy Fuels* 23 (9), 4688–4695. doi:10.1021/ef9003158
- Sang, G., Elsworth, D., Liu, S., and Harpalani, S. (2017). Characterization of Swelling Modulus and Effective Stress Coefficient Accommodating Sorption-Induced Swelling in Coal. *Energy Fuels* 31 (9), 8843–8851. doi:10.1021/acs.energyfuels.7b00462
- Shi, R., Liu, J., Wei, M., Elsworth, D., and Wang, X. (2018). Mechanistic Analysis of Coal Permeability Evolution Data under Stress-Controlled Conditions. *Int. J. Rock Mech. Mining Sci.* 110, 36–47. doi:10.1016/j.ijrmms.2018.07.003
- Somerton, W. H., Söylemezoğlu, I. M., and Dudley, R. C. (1975). Effect of Stress on Permeability of Coal. *Int. J. Rock Mech. Mining Sci. Geomechanics Abstr.* 12, 129–145. doi:10.1016/0148-9062(75)91244-9
- Tanikawa, W., and Shimamoto, T. (2009). Comparison of Klinkenberg-Corrected Gas Permeability and Water Permeability in Sedimentary Rocks. *Int. J. Rock Mech. Mining Sci.* 46, 229–238. doi:10.1016/j.ijrmms.2008.03.004
- van Bergen, F., Pagnier, H., and Krzystalik, P. (2006). Field experiment of Enhanced Coalbed methane-CO₂ in the Upper Silesian basin of Poland. *Environ. Geosci.* 13, 201–224. doi:10.1306/eg.02130605018
- Vandamme, M., Brochard, L., Lecampion, B., and Coussy, O. (2010). Adsorption and Strain: The CO₂-induced Swelling of Coal. *J. Mech. Phys. Sol.* 58, 1489–1505. doi:10.1016/j.jmps.2010.07.014
- Walsh, J. B. (1981). Effect of Pore Pressure and Confining Pressure on Fracture Permeability. *Int. J. Rock Mech. Mining Sci. Geomechanics Abstr.* 18, 429–435. doi:10.1016/0148-9062(81)90006-1
- Walsh, J. B. (1965). The Effect of Cracks on the Compressibility of Rock. *J. Geophys. Res.* 70, 381–389. doi:10.1029/jz070i002p00381
- Wang, C., Zhai, P., Chen, Z., Liu, J., Wang, L., and Xie, J. (2017). Experimental Study of Coal Matrix-Cleat Interaction under Constant Volume Boundary Condition. *Int. J. Coal Geology*, 181, 124–132. doi:10.1016/j.coal.2017.08.014
- Wang, C., Zhang, J., Zang, Y., Zhong, R., Wang, J., Wu, Y., et al. (2021). Time-dependent Coal Permeability: Impact of Gas Transport from Coal Cleats to Matrices. *J. Nat. Gas Sci. Eng.* 88, 103806. doi:10.1016/j.jngse.2021.103806
- Wang, S., Elsworth, D., and Liu, J. (2013). Permeability Evolution during Progressive Deformation of Intact Coal and Implications for Instability in Underground Coal Seams. *Int. J. Rock Mech. Mining Sci.* 58, 34–45. doi:10.1016/j.ijrmms.2012.09.005
- Wang, S., Elsworth, D., and Liu, J. (2011). Permeability Evolution in Fractured Coal: The Roles of Fracture Geometry and Water-Content. *Int. J. Coal Geology*, 87, 13–25. doi:10.1016/j.coal.2011.04.009
- Wu, Y., Liu, J., Elsworth, D., Siriwardane, H., and Miao, X. (2011). Evolution of Coal Permeability: Contribution of Heterogeneous Swelling Processes. *Int. J. Coal Geology*, 88, 152–162. doi:10.1016/j.coal.2011.09.002

- Zang, J., and Wang, K. (2017). Gas Sorption-Induced Coal Swelling Kinetics and its Effects on Coal Permeability Evolution: Model Development and Analysis. *Fuel* 189, 164–177. doi:10.1016/j.fuel.2016.10.092
- Zhang, D., Gu, L., Li, S., Lian, P., and Tao, J. (2013). Interactions of Supercritical CO₂ with Coal. *Energy Fuels* 27 (1), 387–393. doi:10.1021/ef301191p
- Zhou, F., Hussain, F., and Cinar, Y. (2013). Injecting Pure N₂ and CO₂ to Coal for Enhanced Coalbed Methane: Experimental Observations and Numerical Simulation. *Int. J. Coal Geology*. 116–117, 53–62. doi:10.1016/j.coal.2013.06.004
- Zhu, W., Liu, L., Liu, J., Wei, C., and Peng, Y. (2018). Impact of Gas Adsorption-Induced Coal Damage on the Evolution of Coal Permeability. *Int. J. Rock Mech. Mining Sci.* 101, 89–97. doi:10.1016/j.ijrmms.2017.11.007
- Zimmerman, R. W., Chen, D.-W., and Cook, N. G. W. (1992). The Effect of Contact Area on the Permeability of Fractures. *J. Hydrol.* 139, 79–96. doi:10.1016/0022-1694(92)90196-3
- Zimmerman, R. W. (1985). The Effect of Microcracks on the Elastic Moduli of Brittle Materials. *J. Mater. Sci. Lett.* 4, 1457–1460. doi:10.1007/bf00721363

Conflict of Interest: The authors declare that the research was conducted in the absence of any commercial or financial relationships that could be construed as a potential conflict of interest.

Publisher's Note: All claims expressed in this article are solely those of the authors and do not necessarily represent those of their affiliated organizations, or those of the publisher, the editors, and the reviewers. Any product that may be evaluated in this article, or claim that may be made by its manufacturer, is not guaranteed or endorsed by the publisher.

Copyright © 2022 Liu and Spiers. This is an open-access article distributed under the terms of the Creative Commons Attribution License (CC BY). The use, distribution or reproduction in other forums is permitted, provided the original author(s) and the copyright owner(s) are credited and that the original publication in this journal is cited, in accordance with accepted academic practice. No use, distribution or reproduction is permitted which does not comply with these terms.